JOURNAL OF GEOPHYSICAL RESEARCH, VOL. 102, NO. D24, PAGES 29,717–29,727, DECEMBER 26, 1997

Estimation of photosynthetically active radiation absorbed at the surface

Zhanqing Li,[1] Louis Moreau,[2] Josef Cihlar[1]

Abstract. This paper presents a validation and application of an algorithm by *Li and Moreau* [1996] for retrieving photosynthetically active radiation (PAR) absorbed at the surface ($APAR_{SFC}$). $APAR_{SFC}$ is a key input to estimating PAR absorbed by the green canopy during photosynthesis. Extensive ground-based and space-borne observations collected during the BOREAS experiment in 1994 were processed, colocated, and analyzed. They include downwelling and upwelling PAR observed at three flux towers, aerosol optical depth from ground-based photometers, and satellite reflectance measurements at the top of the atmosphere. The effects of three-dimensional clouds, aerosols, and bidirectional dependence on the retrieval of $APAR_{SFC}$ were examined. While the algorithm is simple and has only three input parameters, the comparison between observed and estimated $APAR_{SFC}$ shows a small bias error (<10 W m^{-2}) and moderate random error (36 W m^{-2} for clear, 61 W m^{-2} for cloudy). Temporal and/or spatial mismatch between satellite and surface observations is a major cause of the random error, especially when broken clouds are present. The algorithm was subsequently employed to map the distribution of monthly mean $APAR_{SFC}$ over the 1000 × 1000 km^2 BOREAS region. Considerable spatial variation is found due to variable cloudiness, forest fires, and nonuniform surface albedo.

1. Introduction

The Boreal Ecosystem-Atmosphere Study (BOREAS) is a large international field experiment with the goal of improving the understanding of the exchanges of radiative energy, sensible heat, water, CO_2, and trace gases between the boreal forest and the atmosphere [*Sellers et al.*, 1995]. Photosynthesis is essential in regulating many of the exchange processes. With a sufficient supply of nutrients and water, the photosynthetic rate is governed primarily by the solar energy in the wavelength region 400–700 nm, referred to as photosynthetically active radiation (PAR). Green vegetation can absorb up to 95% of the incident PAR, the bulk of which is converted into latent and sensible heat. Only a small fraction (<5%) is consumed in photochemical processes in which CO_2 is assimilated as organic carbon [*Monteith*, 1972; *Myneni and Ganapol*, 1992]. Therefore the amount of PAR absorbed by green vegetation (APAR) not only influences the net primary productivity and the carbon cycle but also affects the exchange of energy and water between the atmosphere and the land surface.

Monitoring APAR over a large area is a great challenge due to the paucity of ground-based observations. This is true even for a field experiment as large and expensive as BOREAS. Although BOREAS deployed tens of PAR radiometers, they covered only a small portion of the 1000 × 1000 km^2 BOREAS region. In addition, the majority of the stations were equipped only with an up-facing PAR sensor at the top of the tree crowns, while the determination of canopy-absorbed PAR entails simultaneous measurements from four PAR sensors: up-facing and down-facing, placed above and below the tree crowns. There were very few sites with all the components measured. Clearly, mapping APAR cannot be achieved from ground-based observations, and remote sensing is the only feasible alternative.

Remote sensing of APAR has been achieved by estimating surface downwelling PAR ($PAR\downarrow$) and the fraction of PAR intercepted by the canopy (FPAR). $PAR\downarrow$ can be inferred from satellite measurements in visible channels [*Frouin and Gautier*, 1990; *Pinker and Laszlo*, 1992; *Gu and Smith*, this issue] or in other solar channels such as UV [*Eck and Dye*, 1991]. FPAR is usually related to remotely sensed vegetation indices, which are combinations of visible and near-infrared satellite measurements [*Sellers*, 1985; *Goward and Huemmrich*, 1992; *Roujean and Breon*, 1995]. Determination of $PAR\downarrow$ from satellite data requires knowledge of the atmosphere, clouds, and surface, cloud properties being the most critical. In contrast, the PAR absorbed at the surface by the vegetation-soil complex ($APAR_{SFC}$) can be retrieved much more easily, as demonstrated by *Li and Moreau* [1996]. Given $APAR_{SFC}$, PAR albedo, and FPAR, the amount of PAR absorbed by the green canopy can be computed [*Cihlar et al.*, this issue]. Unlike $PAR\downarrow$, inversion of $APAR_{SFC}$ and PAR albedo does not need to specify cloud parameters. The cloud effect is "encoded" in the reflection at the top of the atmosphere (TOA) as measured from satellite platforms [*Li and Moreau*, 1996].

This study deals with $APAR_{SFC}$ only. The paper is structured as follows: Section 2 describes the algorithm of *Li and Moreau* [1996] which forms the basis of the study. The data employed are described in section 3. Section 4 provides analysis of the data and discussion of their characteristics. Validation of the algorithm and mapping of $APAR_{SFC}$ over the BOREAS region are presented in section 5.

[1]Canada Centre for Remote Sensing, Ottawa.
[2]Intermap Information Technologies Ltd., Ottawa.

Paper number 97JD01219.
0148-0227/97/97JD-01219$09.00

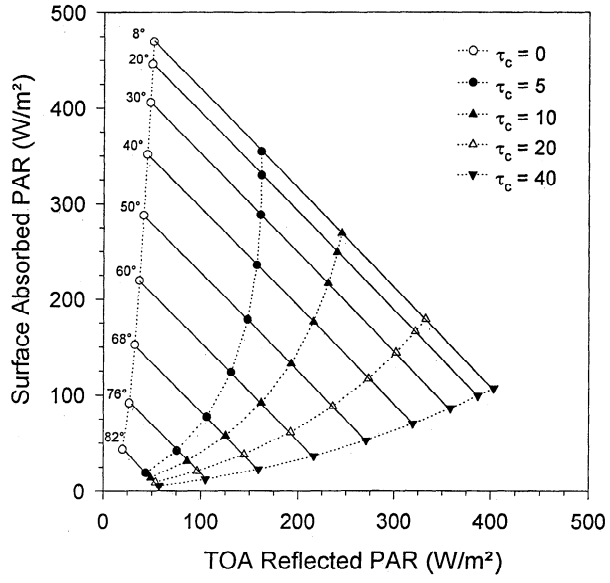

Figure 1. Model relationship between upwelling photosynthetically active radiation (PAR) at the top of the atmosphere (TOA) and $APAR_{SFC}$ (absorbed). Solid curves represent the linear regressions of the simulation results for different cloud optical thicknesses given by τ_c for the same solar zenith angles (SZAs). The simulations are for the midlatitude summer atmosphere with an ozone amount of 0.332 cm atm and a surface albedo of 5% [from *Li and Moreau*, 1996] (reprinted with permission from *Rem. Sens. Environ.*, *55*, 175–191, 1996, Elsevier Science Inc.).

2. Algorithm

The algorithm of *Li and Moreau* [1996] was developed following extensive radiative transfer calculations with a doubling-adding atmospheric radiative transfer model [*Masuda et al.*, 1995] for a range of conditions. The algorithm takes advantage of the linear relationship between $APAR_{SFC}$ and PAR reflected at the TOA ($PAR\uparrow_{TOA}$) for a fixed solar zenith angle (SZA). The relationship is driven by synchronous variations in $APAR_{SFC}$ and $PAR\uparrow_{TOA}$ caused by the changes in cloud optical thickness (compare Figure 1). Because of this, $APAR_{SFC}$ can be predicted from $PAR\uparrow_{TOA}$ without knowledge of the cloud optical thickness. Sensitivity tests [*Li and Moreau*, 1996] suggest that the linear relationship is either weakly dependent on or independent of cloud microphysics, cloud amount, cloud height, and surface albedo. The relationship is altered, however, by the absorbers of PAR, primarily ozone and aerosol. Their effects are accounted for by the following physics-based parameterizations that fit well the results of detailed radiative transfer computations [*Li and Moreau*, 1996]:

$$APAR_{SFC} = a_{PAR}\, PAR\downarrow_{TOA} \tag{1}$$

$$a_{PAR} = \alpha(\mu, O_3, \tau_e) - \beta(\mu, O_3, \tau_e) r_{TOA} \tag{2}$$

$$\alpha(\mu, O_3, \tau_e) = -0.015 + \exp(-0.05 O_3 \mu^{-1}) - 0.168\tau_e[\exp(-3\mu^2) + 1] \tag{3}$$

$$\beta(\mu, O_3, \tau_e) = \exp(0.083 O_3) - 0.168\tau_e(1.21 - 0.348\mu) \cdot [\exp(-3\mu^2) + 1] \tag{4}$$

$$\tau_e = \tau_a[(1 - \omega_a)/0.109]^{0.845} \tag{5}$$

where μ is the cosine of the SZA; O_3 is the amount of ozone in centimeter-atmosphere; τ_a and ω_a are aerosol optical thickness and single-scattering albedo at 550 nm; r_{TOA} is the PAR albedo at the TOA which can be inferred from satellite-observed visible albedo [*Li and Moreau*, 1996]; and a_{PAR} represents surface absorbed PAR normalized by the PAR incident at the TOA, $PAR\downarrow_{TOA}$. Instantaneous and daily mean $PAR\downarrow_{TOA}$ are computed by

$$PAR\downarrow_{TOA} = PAR_o d^{-2} \mu \tag{6}$$

$$PAR\downarrow_{TOA,d} = PAR_o d^{-2} \mu_d f_d \tag{7}$$

where d is the Sun-Earth distance in astronomical units; PAR_O is the incoming PAR at the TOA for the mean Sun-Earth distance ($d = 1$) which is set to be 544 W m^{-2} according to the extraterrestrial solar irradiance data of *Iqbal* [1983]; μ_d is the daytime mean cosine of solar zenith angle; and f_d is the fraction of daytime. Both μ_d and f_d can be computed according to date and latitude.

While the coefficients in the above equations were obtained by fitting the parameterizations to the results of a detailed atmospheric radiative transfer model, the formats of the parameterizations were selected on the basis of radiative transfer rather than through empirical fitting [*Li and Moreau*, 1996]. The first and second terms of the linear relationship given in (2) represent principally the attenuation of downwelling and upwelling PAR, respectively. Therefore α depends only on the amounts of PAR absorbers, while β is modified by both absorbing and scattering events. Note that the parameterization does not include a term accounting for cloud absorption. This is because pure water cloud droplets have almost zero absorption in PAR (<0.2 W m^{-2}; see I in Table 1). However, the cloud does alter moderately the amount of PAR absorbed in

Table 1. Atmospheric Absorption of PAR (W m^{-2}) Computed With a Douling-Adding Radiative Transfer Model [*Masuda et al.*, 1995] Under Different Atmospheric and Cloud Conditions at Various Cosines of Solar Zenith Angle μ

μ	0.011	0.056	0.135	0.240	0.365	0.500	0.635	0.760	0.865	0.944	0.989
I	0.00	0.00	0.01	0.02	0.03	0.05	0.06	0.08	0.10	0.12	0.13
II	1.54	6.07	10.03	12.58	14.39	15.84	17.05	18.06	18.85	19.41	19.73
III	1.50	6.05	10.30	13.55	16.38	19.07	21.63	23.96	25.91	27.36	28.21
IV	−0.04	−0.02	0.27	0.97	1.99	3.23	4.58	5.90	7.06	7.95	08.48
V	1.85	8.32	16.58	24.72	32.49	40.03	47.26	53.90	59.56	63.81	66.29

PAR, photosynthetically active radiation. I, absorption by cloud droplets only; the atmosphere used contains no ozone and aerosol. II, Clear midlatitude summer atmosphere [*McClatchey et al.*, 1971] with a surface albedo of 20%. III, Same atmosphere as in II but including a stratocumulus cloud [*Stephens*, 1979] of optical thickness 80 in 2–4 km. IV, Difference between III and II (III − II). V, Same atmosphere and cloud as in III except that (1) the cloud is placed in 0–1 km and (2) a continental aerosol [*WCP*, 1986] of optical thickness 0.225 is included.

the entire atmospheric column by serving as a reflector, which provides more PAR photons to be captured by the PAR absorbers, such as ozone or aerosols. This is clearly seen from the comparison of atmospheric PAR absorption under clear (II in Table 1) and cloudy (III) conditions. Their difference (IV) is significantly larger than the cloud absorption (I). As a result, the increase in absorption is generally accompanied by an increase in TOA reflection. This coupling relationship is exploited in the algorithm [*Li and Moreau*, 1996]. Nevertheless, the algorithm may suffer significant uncertainties when cloud droplets and absorbing aerosols (e.g., fire smoke) are located in the same layer. In particular, black carbon contained in fire smokes can drastically enhance PAR absorption (see V in Table 1) and at the same time reduces cloud reflection.

The above algorithm, while extremely simple, can reproduce accurately the results of a much more complex radiative transfer model under a variety of conditions [*Li and Moreau*, 1996]. The $APAR_{SFC}$ estimated with the algorithm agreed to within ± 5 W m^{-2} of the model results for 93% of the cases representing a wide range of combinations of clouds, aerosols, and surfaces. Furthermore, a preliminary validation using instantaneous observations obtained during the First International Satellite Land Surface Climatology Project (ISLSCP) Field Experiment (FIFE) data showed a bias error of 3 W m^{-2} and a standard error of 22 W m^{-2} [*Li and Moreau*, 1996]. For the algorithm to be applied for mapping $APAR_{SFC}$ over the BOREAS region, further validation is needed due to its distinct environment.

3. Data

The data employed for this study were acquired as part of the BOREAS project, which was conducted in the boreal forest region of central Canada [*Sellers et al.*, 1995]. Satellite data were obtained over the BOREAS region encompassing most of Saskatchewan and Manitoba. Ground-based measurements were made primarily in two BOREAS study areas, northern (NSA) and southern (SSA), which are approximately 8000 km^2 each and are separated by about 500 km.

Complex infrastructure and a variety of instruments were deployed throughout each study area. Of particular interest here are three flux towers (TF03, TF08, and TF09) at which both upwelling and downwelling PAR fluxes were measured and made available through the BOREAS Information System (BORIS). The towers were located near the centers of relatively homogeneous areas $\geq$1 km^2. All radiation sensors were mounted near the tops of the towers, well above the top of the canopy. TF03 was located at a mature black spruce site in the NSA (NOBS; 55.879°N, 98.484°W). TF08 was placed at a mature jack pine site in the NSA (NOJP; 55.927°N, 98.624°W). TF09 was an OBS tower located in SSA (SOBS; 53.985°N, 104.691°W). Thirty-minute mean PAR data were provided to the BORIS. TF03 also included the standard deviations of PAR measurements which we used to evaluate the effects of broken clouds. The data periods are October 4, 1993 to December 4, 1994 for NOBS, May 24 to September 20, 1994 for NOJP, and May 23 to September 21, 1994 for SOBS.

Aerosol was monitored by a network of six automatic Sun photometers distributed across the BOREAS region. Aerosol optical thickness was retrieved at six spectral intervals (339, 380, 441, 672, 873, and 1022 nm) with estimated uncertainties around 0.02 for spectral bands above 400 nm. The data at 441 and 672 nm were linearly interpolated to obtain aerosol optical thickness at 550 nm for use in the $APAR_{SFC}$ model. The aerosol data archived in BORIS span the period May 18 to November 1, 1994 for the NSA and May 23 to October 10 for the SSA. They are only available under clear-sky conditions. Clear/cloud discrimination was based on the temporal variation of incident irradiance and spectral variation of optical thickness (B. Markham, personal communication, 1996). Under cloudy conditions, aerosol optical thickness was taken from the nearest clear-sky measurement if available within 12 hours. Since no information is available regarding aerosol optical properties, a continental type of aerosol was assumed [*World Climate Program* (*WCP*), 1986].

Ozone amount is also required as input into the $APAR_{SFC}$ model. Compared to aerosol, the effect of ozone on the retrieval of $APAR_{SFC}$ is small [*Li and Moreau*, 1996]. Moreover, for a given region and season the ozone amount is much more stable than for aerosol. Therefore we used a constant value of 300 Dobson units in our calculations.

Satellite data were obtained by the advanced very high resolution radiometer (AVHRR) onboard NOAA 11. Reflectance measurements in channels 1 (570–680 nm) and 2 (710–980 nm) were employed. Because of the overlap of satellite orbits at high latitudes, multiple daytime measurements were available between 1500 and 1800 LT. Daily AVHRR data were acquired in Prince Albert, Saskatchewan, Canada, and processed by the Manitoba Remote Sensing Centre using the geocoding and compositing (GEOCOMP) system [*Robertson et al.*, 1992]. GEOCOMP performs sensor calibration, geometric registration, and resampling. Time dependent gains and offsets [*Cihlar and Teillet*, 1995] were used for sensor calibration. The satellite images were registered using image chips and resampled to uniform 1 km^2 pixels. Since the AVHRR measures reflectance from a single viewing direction and the algorithm requires albedo defined over the entire upper hemisphere, angular corrections were needed. To this end we employed the bidirectional model of *Wu et al.* [1995] and *Li et al.* [1996] for clear-sky measurements, and the model developed for the Earth Radiation Budget Experiment (ERBE) [*Suttles et al.*, 1988] for cloudy image data.

After all the data essential for validation were assembled, they were matched in space and time. The most delicate and time-consuming step was to locate the towers on an AVHRR image. With the aid of an image processing software (PCI), we were able to find the tower locations with a precision 1–2 pixels. Since the PAR data are averages over time, temporal matching error is up to 30 min, which may pose a problem for evolving clouds. Time difference with respect to aerosol data could be much longer, since aerosol data were only available during clear periods.

4. Analysis

Figure 2 presents PAR $\downarrow$ flux and transmissivity measured at the three flux towers as well as the standard deviations of PAR $\downarrow$ flux measured at the NOBS. Atmospheric transmissivity was computed as the ratio of the PAR incident at the surface (above canopy) and at the TOA. Only the data matched with AVHRR measurements are shown here. The unit of measurements has been converted from PAR photon flux (micromol m^{-2} s^{-1}) to PAR energy flux (W m^{-2}). A conversion factor of 4.6 was determined from simulations with a radiative transfer model [*Masuda et al.*, 1995] by incorporating the response function of the PAR sensors under various sky

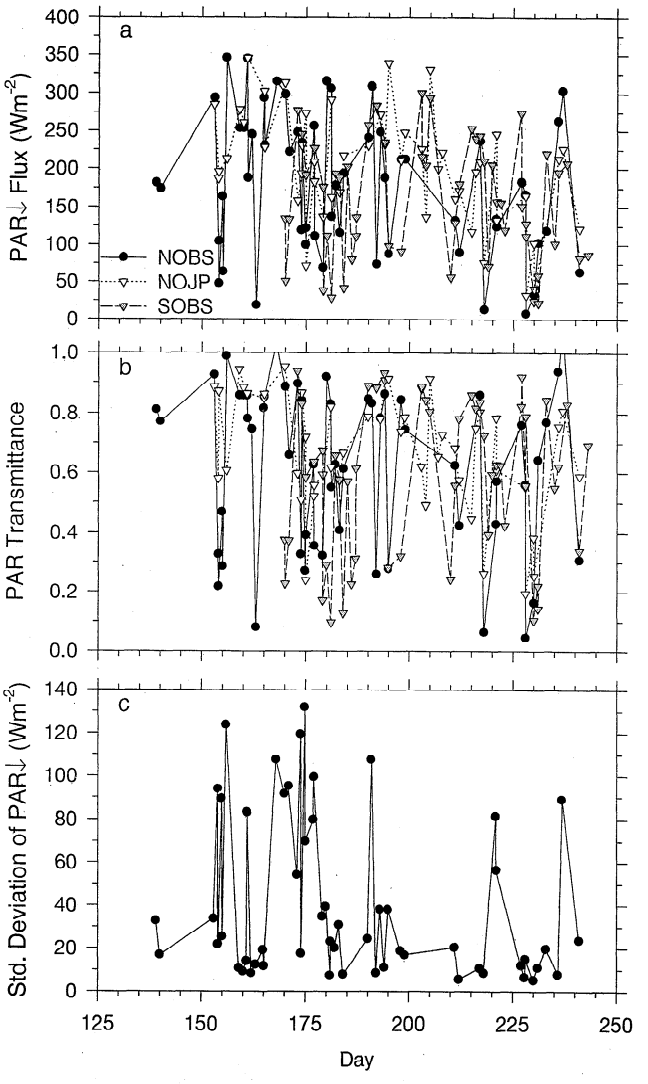

Figure 2. (a) Downwelling PAR flux and (b) PAR transmittance observed at three flux towers (NOBS, NOJP, and SOBS) that were matched with advanced very high resolution radiometer (AVHRR) data. (c) Standard deviation of downwelling PAR flux for NOBS.

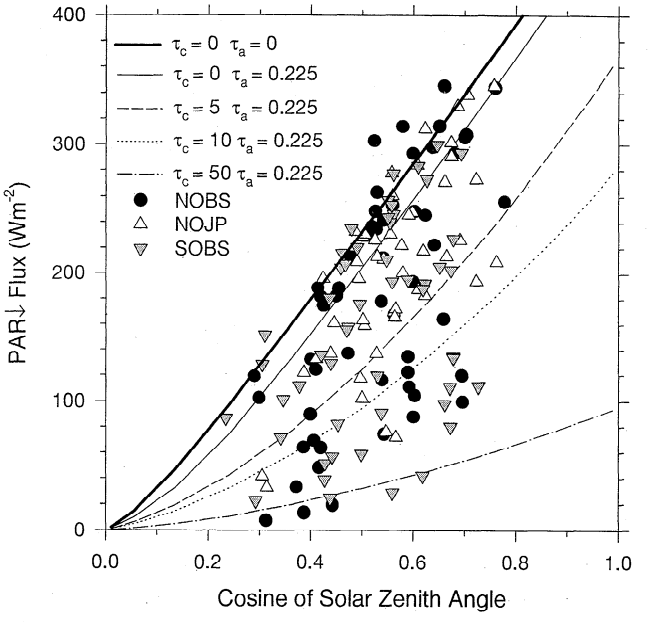

Figure 3. Model-observation comparison of the variation of downwelling PAR with solar zenith angle and cloud optical thickness (τ_c). Aerosol optical thickness is specified by τ_a.

conditions. The conversion factor was found to vary only slightly with changes in cloud and aerosol (Table 2). From Figure 2 it is evident that both PAR flux and PAR transmissivity vary considerably. Downwelling PAR ranged from less than 25 W m^{-2} to about 350 W m^{-2}, and PAR transmissivity varied from less than 0.1 to nearly unity. One measurement even shows transmittance larger than 1.0. While this might be a bad number due to errors in observation or calibration, transmittance larger than 1.0 could happen occasionally if the radiometer was exposed to direct sunlight and, at the same time, received a significant amount of additional photons reflected from the edges of broken clouds. The high-frequency variation in PAR flux and transmissivity is probably caused by convective clouds that occur frequently in the summer. The convective clouds are usually spatially inhomogeneous and temporally variable, making it difficult to match satellite and surface measurements. Temporal variation is indicated by the standard deviation which displays two clusters separated at approximately 50 W m^{-2} (Figure 2b). The top cluster corresponds to fast-evolving clouds.

In addition to cloud amount, cloud optical depth (τ_c) and SZA also modify significantly PAR flux. This can be seen from Figure 3, which shows the variations of PAR ↓ with the two factors. The curves were obtained from model simulation for the midlatitude summer atmosphere [*McClatchey et al.*, 1971] over a vegetated land [*Masuda et al.*, 1995] with cumulus clouds [*Stephens*, 1979] of τ_c ranging from 0 (clear sky) to 50. Aerosol optical thickness (τ_a) was set to 0.225 for all the curves except the solid thick one, which represents a clears-sky ($\tau_c = 0$) condition without any aerosol loading ($\tau_a = 0$). It thus denotes the maximum theoretical bound for PAR ↓. Most observations fall within this limit except for a few points which may be due to the effect of partial clouds. For an overcast cloud, change in PAR at a fixed SZA is mainly controlled by τ_c. The majority of the observations have cloud optical thick-

Table 2. Variation of Factor Used to Convert PAR Photon Flux (micromol m^{-2} s^{-1}) Into PAR Energy Flux (W m^{-2}) With Cloud and Aerosol (Continental Type) Optical Thickness Simulated by a Radiative Transfer Model [*Masuda et al.*, 1995]

μ	0.011	0.056	0.135	0.240	0.365	0.500	0.635	0.760	0.865	0.944	0.989
I	4.60	4.67	4.67	4.66	4.65	4.64	4.64	4.64	4.63	4.63	4.63
II	4.54	4.58	4.64	4.66	4.66	4.65	4.65	4.64	4.64	4.64	4.64
III	4.47	4.51	4.55	4.58	4.59	4.59	4.60	4.60	4.60	4.60	4.60

I, a clear atmosphere (same as II in Table 1). II, Same atmosphere as I but include a continental aerosol of optical thickness 0.225. III, Same atmosphere and aerosol as II but include a cloud of optical thickness 50.

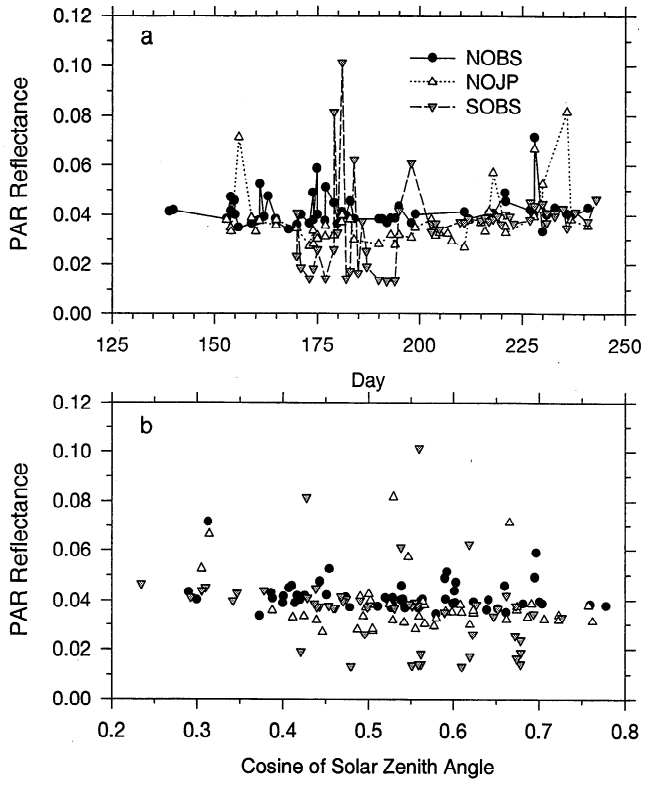

Figure 4. PAR albedo observed at the top of three flux towers (NOBS, NOJP, and SOBS) as functions of (a) date and (b) the cosine of solar zenith angle.

ness less than 50, although a few could be much higher, as PAR ↓ approaches asymptotic value at high τ_c. The large impact of SZA on PAR ↓ is readily understandable. The wide range of SZA implies that the results of validation may be valid for many seasons.

Surface PAR albedo is defined as the ratio of upwelling and downwelling PAR fluxes measured above the canopy. Its seasonal variation and dependence on the SZA are shown in Figure 4. For NOBS and NOJP, PAR albedo was quite stable at about 0.04 and increased slightly with an increasing SZA. The SOBS data exhibit an unusually strong fluctuation, although the mean value was close to the other two sites. Since variations up to a factor of 5 occur within a very short time period at similar solar zenith angles, they are unlikely to represent real physical changes of the scene. The presence of noise in the data is an important consideration for the validation.

Figure 5 presents aerosol optical thickness on the days when both surface and satellite data were available. It is clear that the magnitude and variation of aerosol loading were so large that accounting for this effect is essential. The aerosol episodes were caused by forest fires. In the summer of 1994 there were many fires around the BOREAS region [*Li et al.*, this issue]. Heavy smoke was visible when aerosol optical thickness was above 0.5 (B. Markham, private communication, 1997). The smoke can attenuate considerably the amount of PAR reaching the ground [*Sellers et al.*, 1995] due to both scattering and absorption. The single-scattering albedo for biomass burning aerosols varies from 0.7 (extremely strong absorption) to near unity (almost no absorption) [*Lenoble*, 1991]. Unfortunately, lack of chemical composition and aerosol size distribution in the BOREAS measurements do not allow us to compute the exact values of the single-scattering albedo. Therefore the continental aerosol defined in WCP-112 [*WCP*, 1986] was

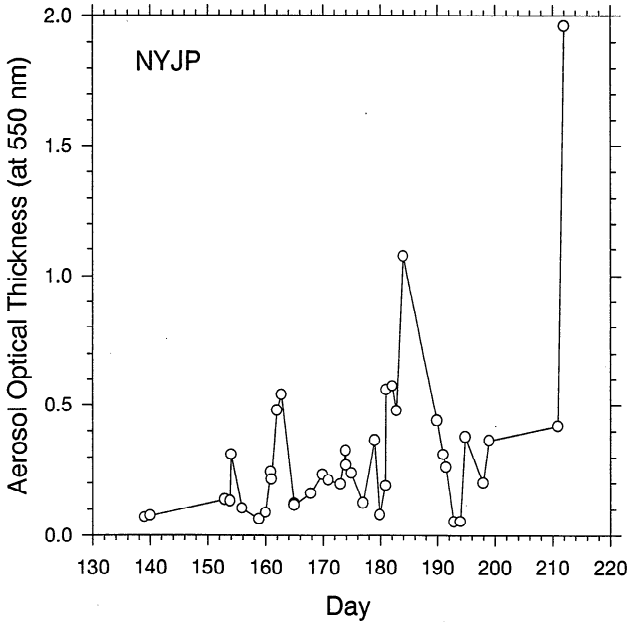

Figure 5. Variation of aerosol optical thickness at 550 nm in the summer of 1994 in the BOREAS northern study area.

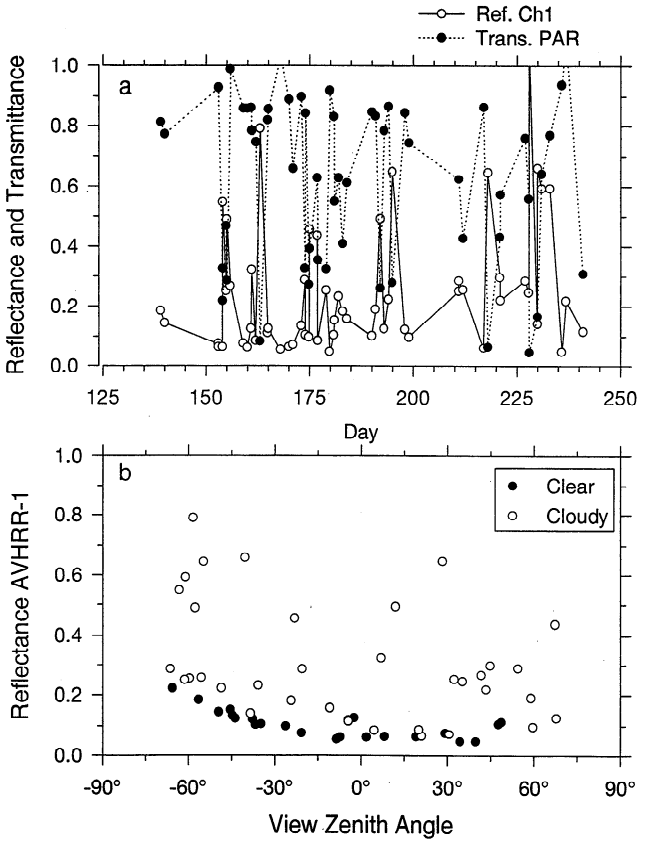

Figure 6. Variation of AVHRR channel 1 reflectance with date and viewing zenith angle over the NOBS in the summer of 1994. Open and solid circles correspond to cloudy and clear measurements.

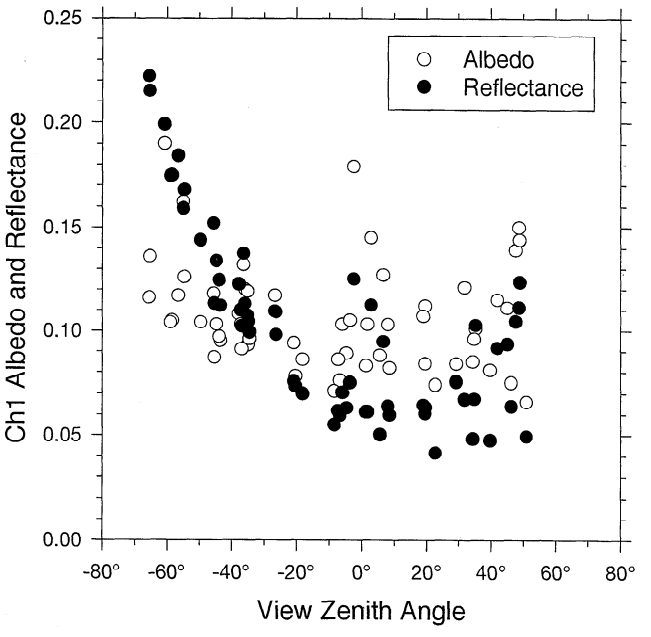

Figure 7. Comparison of clear-sky AVHRR channel 1 reflectance and albedo. The latter was obtained following a bidirectional correction described in the Appendix.

adopted. It has a single-scattering albedo close to the median value for biomass burning aerosols in visible wavelength [*Kaufman et al.*, 1994].

Figure 6 shows reflectance measurements in AVHRR channel 1 which were matched with ground observations. As a gross check of the correspondence between satellite and surface observations, PAR transmittance is also plotted. As expected, the two quantities covary but are out of phase (Figure 6a). The reflectance is also plotted with respect to AVHRR viewing zenith angle (VZA) (Figure 6b). Positive and negative VZAs represent forward and backscattering directions, respectively. The data were classified as being clear (cloudy) if the ratio of channel 2 over channel 1 reflectance was larger (smaller) than 1.63. This threshold was based on a visual analysis of a large number of AVHRR images acquired in the BOREAS region during the summer of 1994. Figure 6b exhibits a strong bidirectional effect, especially for clear-sky measurements. Reflection at extreme backscattering angles exceeds that at nadir by a factor of 3–4, which would lead to unacceptably large errors if the Lambertian assumption were made. Clear-sky albedos were therefore derived following a bidirectional correction (refer to the Appendix). Figure 7 compares the reflectance and albedo. In contrast to reflectance, albedo shows only a minor trend with respect to the VZA. Note that the correction does not remove the dependence of albedo on SZA. Although the angular effect for cloudy measurements was not so strong as for clear sky, it was not negligible.

5. Validation and Mapping

After preprocessing, the various input data were substituted into (1)–(7) to estimate $APAR_{SFC}$ to be compared with $APAR_{SFC}$ values observed at the towers. Figure 8 presents comparisons for three cases at the NOBS (TF03): clear, overcast and broken clouds. As mentioned earlier, clear/cloudy discrimination was made according to the ratio of reflectance in channels 2 and 1, while broken/overcast clouds were separated by the standard deviation of measured downwelling PAR during a 30-min period. The standard deviation (sd) of the differences between observed (30-min mean) and estimated $APAR_{SFC}$ (instantaneous) vary significantly among the three categories: largest for broken clouds (95.9 W m^{-2}), moderate for overcast (47.9 W m^{-2}), and lowest for clear sky (17.8 W m^{-2}).

The strong dependence of sd on cloud inhomogenity and mobility indicates that the scatter in Figure 8 stems mainly

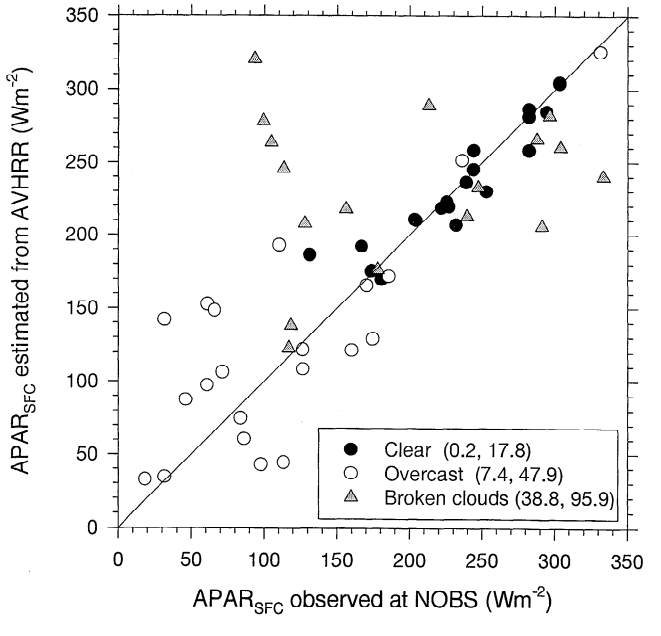

Figure 8. Comparison between observed and estimated $APAR_{SFC}$ for the NOBS under clear, overcast and broken cloud conditions. The first and second numbers in the parentheses represent the mean and standard differences (sd) between observed and estimated $APAR_{SFC}$.

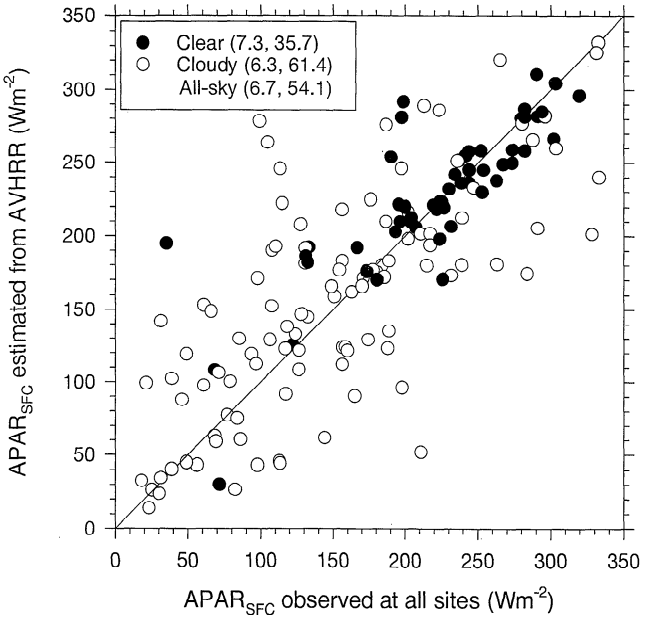

Figure 9. Same as Figure 8 but for all the three towers under study (NOBS, NOJP, and SOBS). The data are differentiated into clear and cloudy.

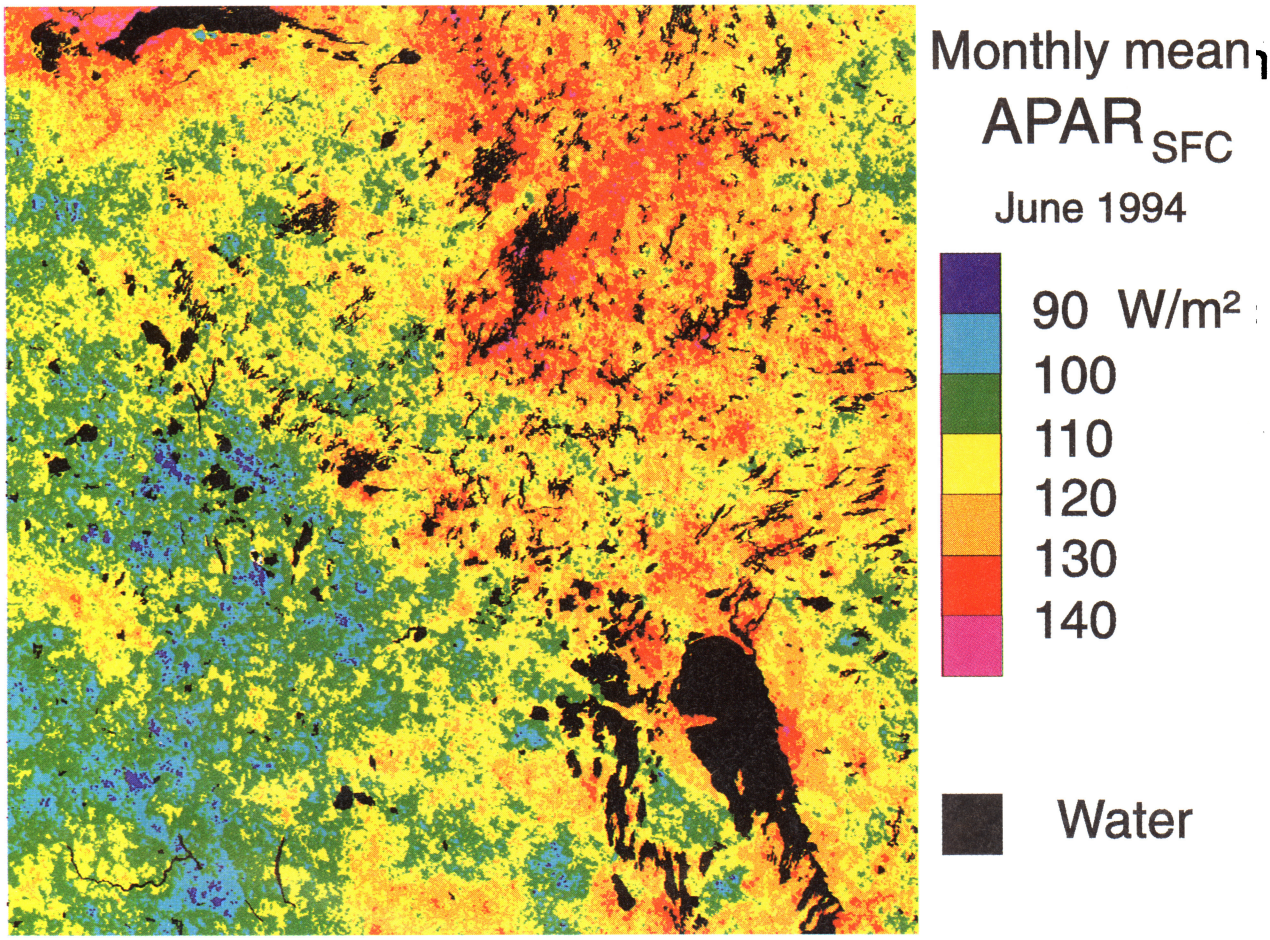

Plate 1. Distribution of monthly mean $APAR_{SFC}$ estimated from AVHRR in the BOREAS region in June 1994. It covers an area of 1000 × 1000 km^2, centered around 55°13′41″N and 103°6′53″W, with the Lambert conformal conic projection.

from the mismatch between satellite and surface observations in time and/or in space. Although the satellite and tower measurements were colocated carefully, large discrepancies due to spatial match are inevitable in case of broken clouds. This is because unlike satellite measurements, which represent a small field of view, an upward facing PAR sensor at the surface measures incoming PAR photons from all directions. When the sky is covered partially by clouds, the space and surface views may thus differ considerably. Therefore sd is the upper limit of the random error in the estimates of $APAR_{SFC}$, not its actual value. When multiple samples are averaged, the sd for the averaged quantities should decrease with the number of samples included. Consequently, the real random error in the monthly mean estimates of $APAR_{SFC}$ is expected to be much lower than the sd values shown in Figure 8. The mean differences (md) were equal to 38.8, 7.4, and 0.2 W m^{-2} for broken clouds, overcast, and clear-sky comparisons, respectively (Figure 8). Note that these values are also influenced statistically by sd. At the 95% confidence level, the true mean bias error falls within the range of Δmd that is determined by both sd and sample number (N),

$$\Delta md = 1.96 \frac{sd}{\sqrt{N}}. \quad (8)$$

Δmd is found to be 58.3, 25.7, and 10.5 W m^{-2}, respectively, for broken clouds, overcast, and clear skies. The absence of standard deviation data prevents a similar analysis for the NOJP and SOBS towers. An overall comparison using data from all three towers is presented in Figure 9. Again, scattering of the clear data points around the 1:1 line is significantly less than that for the cloudy ones, while their mean differences with respect to the surface observations are about the same.

It should be noted that mismatch between satellite and surface measurements is not the sole cause for the discrepancy between the observed and estimated $APAR_{SFC}$. For example, the large uncertainties in some PAR albedo measurements at the SOBS discussed earlier (compare Figure 4) can produce a discrepancy in $APAR_{SFC}$ shown in Figure 9. Imperfect algorithm and corrections for aerosol and bidirectional effects are also among the potential sources of uncertainty. The largest potential uncertainty is likely to occur when smoke and clouds coexist, as inferred from the sensitivity tests presented in Table 1. Unfortunately, the available information is not sufficient to study this condition experimentally.

By combining tower and satellite observations, we derived daily and monthly mean $APAR_{SFC}$ over the BOREAS region in 1994 in three steps. First, the available NOAA 11/AVHRR

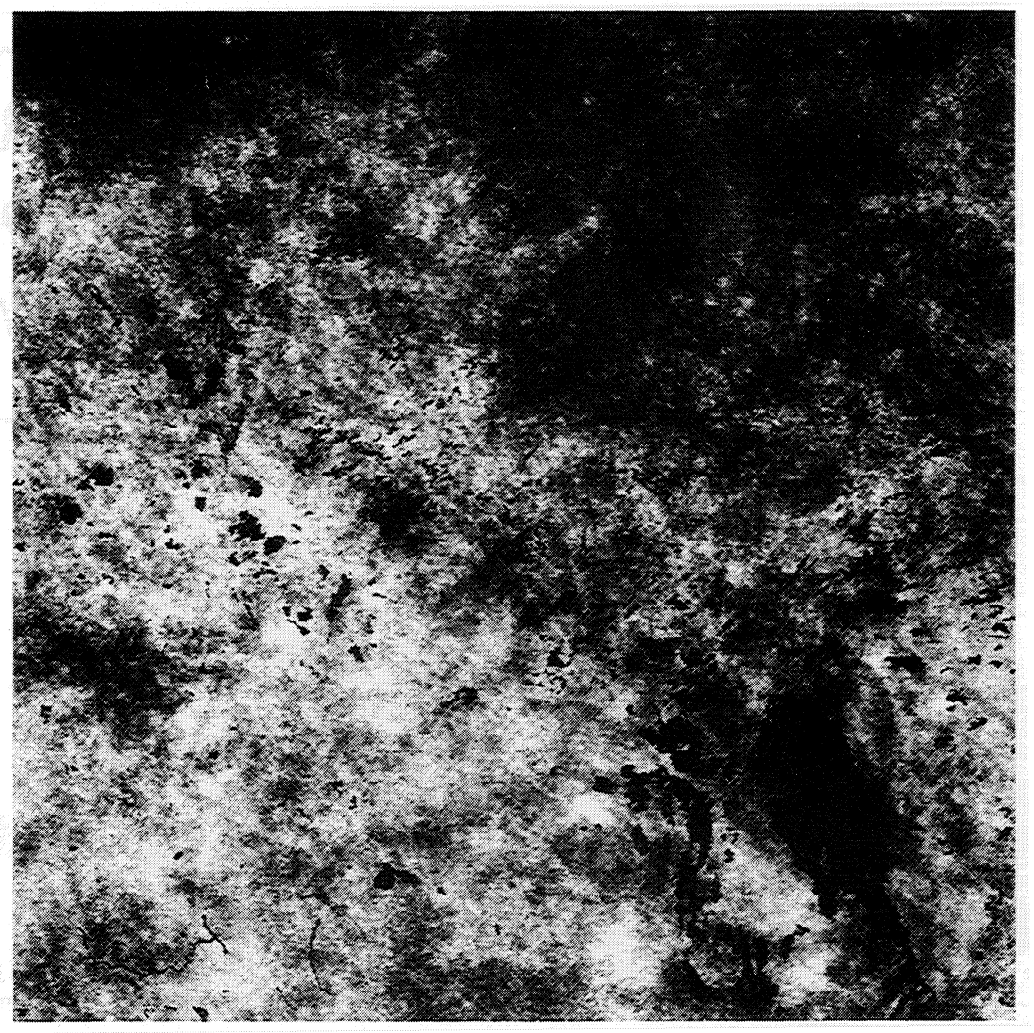

Figure 10. Difference between monthly mean and minimum TOA albedo obtained from daily AVHRR channel 1 images in June 1994. Image brightness is proportional to the difference.

images acquired in the vicinity of the BOREAS region were processed by the GEOCOMP system. The processed data contain calibrated radiances in the five AVHRR channels, VZA, SZA, and relative azimuth angle. A daily composite image over the BOREAS region was constructed from the individual images, by retaining pixels with the lowest VZA in overlapping areas. Bidirectional correction was applied following the method described in the Appendix. Water bodies were masked using the land cover map of *Pokrant* [1991] and excluded from further processing. Instantaneous $APAR_{SFC}$ fluxes were then computed according to (1)–(7) from which daily mean values were derived. Because of inadequate diurnal sampling by the NOAA satellite, continuous tower measurements were employed to characterize the diurnal evolution of $APAR_{SFC}$. From the tower measurements the ratio of instantaneous and daily mean $APAR_{SFC}$, $a_{PAR}(t)$, was computed as a function of local solar time t. Using this function, $R(t)$, the time of satellite overpass, t, a daily mean $APAR_{SFC}$, $APAR_{SFC,d}$ was computed as

$$APAR_{SFC,d} = a_{PAR}(t)\,R(t)\,PAR\downarrow_{TOA,d}. \quad (9)$$

where a_{PAR} is the instantaneous $APAR_{SFC}$ normalized by the TOA incident PAR (compare (2)). Daily mean incident PAR at the TOA, $PAR\downarrow_{TOA,d}$ was calculated by (7).

Plate 1 shows the distribution of monthly mean $APAR_{SFC}$ over the BOREAS region in June 1994. The spatial variation of $APAR_{SFC,d}$ is strong, ranging from less than 90 W m^{-2} in the southwest of the region to larger than 140 W m^{-2} around Reindeer Lake (north) and Lake Athabasca (northwest). To understand the causes of the variation, the difference between monthly mean and minimum TOA albedos observed during the same month is presented in Figure 10. Minimum TOA albedo (i.e., the lowest albedo observed by the satellite) is taken as the nominal clear-sky albedo. The mean-minimum difference is thus a proxy for cloudiness, while the minimum albedo is closely related to clear-sky surface albedo. Plate 1 bears a close resemblance to Figure 10 in spatial distribution, implying that the spatial changes in $APAR_{SFC,d}$ are primarily due to the spatial variation in cloud cover. Nevertheless, the impact of surface albedo on $APAR_{SFC,d}$ is discernible by comparing the minimal TOA albedo (Figure 11) and $APAR_{SFC,d}$ (Plate 1). The large-scale variation in $APAR_{SFC,d}$ is similar to Figure 11. For example, the agricultural land in the southwest has the highest TOA albedo and the lowest $APAR_{SFC,d}$. The effects of increasing solar zenith angle and increasing daytime duration with latitude compensate for each other, resulting in a weak latitudinal $APAR_{SFC,d}$ trend.

Inadequate diurnal sampling is a major limitation to the use

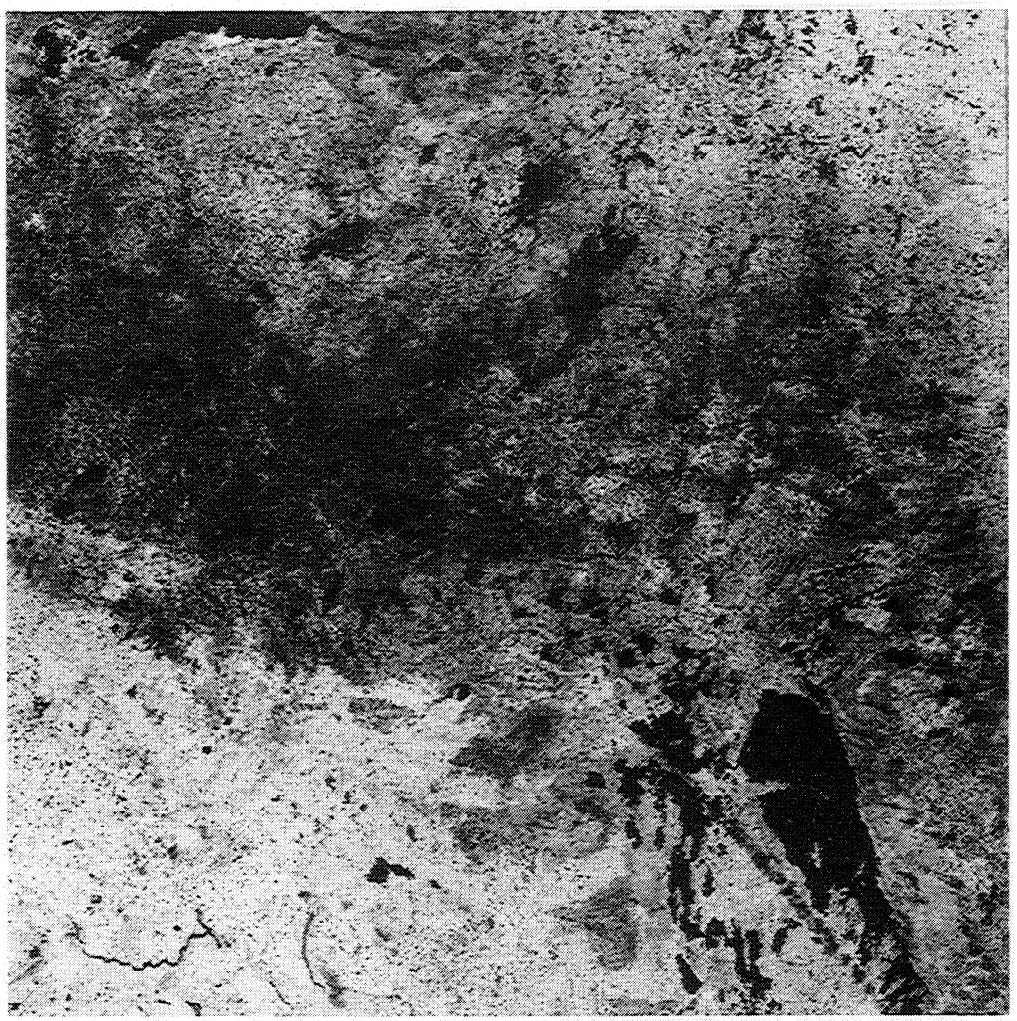

Figure 11. Same as Figure 10 but for minimum AVHRR channel 1 albedo.

of AVHRR for mapping daily APAR. The assumption that the diurnal variation observed at tower sites represent the variations at other locations contains unknown errors which may vary from one location to another. The diurnal sampling problem can be dealt with using geostationary satellite data from GOES [*Gu and Smith*, this issue]. It should be noted that the $APAR_{SFC}$ methodology used here is applicable to any optical satellite measurements, including geostationary ones. The validation tests carried out here indicate that this approach yields a sound estimate of instantaneous $APAR_{SFC}$. Since these tests only assumed accurate satellite sensor calibration, the instantaneous surface-satellite comparisons presented here can also be considered as validation for other optical satellite sensors, provided that the latter are calibrated. In the case of geostationary satellites the spatial resolution and large VZA are the main limitations to their use for vegetation monitoring at northern latitudes.

6. Summary

This study tests and applies a satellite-based algorithm for retrieving photosynthetically active radiation (PAR) absorbed at the surface ($APAR_{SFC}$). Most of the parameters contained in the inversion algorithm were measured during the BOREAS, including visible albedo at the top of the atmosphere (TOA), aerosol optical thickness, solar zenith angle, and upwelling and downwelling PAR fluxes observed at the flux towers. Satellite measurements of the TOA reflectance were acquired by the advanced very high resolution radiometer (AVHRR) onboard NOAA 11. Surface PAR observations were made at three flux towers located in three mature forest stands, namely, TF03, TF08, and TF09. Aerosol optical thickness was derived from photometers deployed across the BOREAS region. The acquired data were matched in time and in space and subjected to various corrections and quality assurance steps. Particular attention was paid to the impact of three-dimensional clouds, cloud optical thickness, and the bidirectional dependence of reflectance on viewing geometry. Comparisons between estimated and observed instantaneous $APAR_{SFC}$ showed small mean and large random differences (see Table 3 for summarized comparison statistics). Random discrepancy was caused by the mismatch between space-borne and surface-based observations under partial cloudy conditions. In principle, it may also result from enhanced PAR absorption by cloud droplets containing black carbon due to forest fires. Daily AVHRR data in 1994 were processed for mapping daily and monthly mean APAR over the BOREAS region. The sampling problem in deriving daily mean $APAR_{sfc}$ from a single satellite observation was overcome by taking

Table 3. Summary of Statistics for Comparisons Between Estimated and Observed $APAR_{SFC}$

	Site								
	NOBS			NOJP		SOBS		All Sites	
Sky Condition	CLR	BCD	OVC	CLR	CLD	CLR	CLD	CLR	CLD
md, W m^{-2}	0.2	7.4	38.8	−1.8	−9.3	25.5	2.5	7.3	6.3
sd, W m^{-2}	17.8	47.9	95.9	32.0	44.9	51.2	58.9	35.7	61.4

md, mean difference; sd, standard difference; CLR, clear sky; BCD, broken clouds; OVC, overcast; CLD, cloudy.

advantage of the frequent ground-based observations. The resulting monthly mean $APAR_{sfc}$ in the BOREAS region of 1000×1000 km^2 shows a considerable spatial variation, with the largest value greater than 140 W m^{-2} and the smallest near 90 W m^{-2}. The variation is caused mostly (1) by nonuniform cloud distribution, (2) by variable surface albedo, and (3) by other factors such as solar zenith angle and daytime length.

Appendix: Derivation of Albedo From Bidirectional AVHRR Reflectance Measurements

The bidirectional effect, as discussed in the main text, was corrected following a method described by *Wu et al.* [1995] and *Li et al.* [1996], which is outlined briefly here.

The first step is to fit clear-sky reflectance observations by the following equation:

$$R_i(\theta_s, \theta_v, \phi) = k_o + a_1(\text{NDVI})k_1 f_1(\theta_s, \theta_v, \phi) + a_2(\text{NDVI})k_2 f_2(\theta_s, \theta_v, \phi) \quad \text{(A1)}$$

where f_1 and f_2 are functions of three geometric angles, namely, solar zenith (θ_s), viewing zenith (θ_v), and relative azimuth (ϕ) [*Roujean et al.*, 1992]; a_1 and a_2 are land-cover dependent functions of normalized difference vegetation index (NDVI) [*Wu et al.*, 1995]. For forest, $a_1 = 0$ and a_2 is a function of NDVI. Using the clear data shown in Figure 6, k_o and k_2 were determined to be 0.0633 and 0.1657, respectively. A modified bidirectional reflectance distribution function (BRDF) is obtained as

$$\Omega(\theta_s, \theta_v, \phi) = 1 + k_2/k_o a_2(\text{NDVI}) f_2(\theta_s, \theta_v, \phi) \quad \text{(A2)}$$

Using this BRDF, TOA albedo defined over the entire upper hemisphere $A(\theta_s)$ is computed as

$$A(\theta_s) = \frac{R(\theta_s, \theta_v, \phi)}{\pi\Omega(\theta_s, \theta_v, \phi)} \cdot \int_0^{2\pi}\int_0^{\pi/2} \Omega(\theta_s, \Theta_v, \Phi)\cos\Theta_v \sin\Theta_v \, d\Theta_v \, d\Phi. \quad \text{(A3)}$$

Acknowledgments. We are very grateful to the BOREAS science team members of TF03 (PI: S. Wofsy, Harvard University), TF08 (PI: D. Fitzjarrald, State University of New York at Albany), TF09 (PI: P. Jarvis, University of Edinburgh), and RSS-11 (PI: B. Markham, NASA GSFC) for collecting and processing data used in the study. The data were archived and made available by the BOREAS Information System (BORIS) designed and maintained by a group at the NASA Goddard Space Flight Center (http: //boreas.gsfc.nasa.gov). B. Holben (NASA GSFC) and E. Smith (Florida State University) carefully reviewed the original manuscript. Discussions with J. Chen (CCRS) and B. Markham are very much appreciated.

References

Cihlar, J., and P. M. Teillet, Forward piecewise linear model for quasi-real time processing of AVHRR data, *Can. J. Remote Sens.*, *21*, 22–27, 1995.

Cihlar, J., J. Chen, and Z. Li, Seasonal AVHRR multichannel data sets and products for studies of surface-atmosphere interactions, *J. Geophys. Res.*, this issue.

Eck, T. F., and D. G. Dye, Satellite estimation of incident photosynthetically active radiation using ultraviolet reflectance, *Remote Sens. Environ.*, *38*, 135–146, 1991.

Frouin, R., and C. Gautier, Variability of photosynthetically available and total solar irradiance at the surface during FIFE: A satellite description, in *Proceedings of the 1st ISLSCP Symposium on Field Experiments*, pp. 98–104, Am. Meteorol. Soc., Boston, Mass., 1990.

Goward, S. N., and K. F. Huemmrich, Vegetation canopy PAR absorptance and the normalized difference vegetation index: An assessment using the SAIL model, *Remote Sens. Environ.*, *39*, 119–140, 1992.

Gu, J., and E. Smith, High-resolution estimates of total solar and PAR surface fluxes over large-scale BOREAS study area from GOES measurements, *J. Geophys. Res.*, this issue.

Iqbal, M., *An Introduction to Solar Radiation*, 390 pp., Academic, San Diego, Calif., 1993.

Lenoble, J., The particulate matter from biomass burning: A tutorial and critical review of its radiative impact, in *Global Biomass Burning: Atmospheric, Climatic, and Biospheric Implications*, edited by J. S. Levine, pp. 381–386, MIT Press, Cambridge, Mass., 1991.

Li, Z., and L. Moreau, A new approach for the remote sensing of canopy absorbed photosynthetically active radiation, I, Total surface absorption, *Remote Sens. Environ.*, *55*, 175–191, 1996.

Li, Z., J. Cihlar, X. Zhang, L. Moreau, and L. Hung, Detection and correction of the bidirectional effect in AVHRR measurements over northern regions, *IEEE Tran. Geosci. Remote Sens.*, *34*, 1308–1322, 1996.

Li, Z., J. Cihlar, L. Moreau, F. Huang, and B. Lee, Monitoring fire activities in the boreal ecosystem, *J. Geophys. Res.*, this issue.

Kaufman, Y. J., D. Tanre, and D. E. Ward, Remote sensing of biomass burning in the Amazon, *Remote Sens. Rev.*, *10*, 51–90, 1994.

Masuda, K., H. G. Leighton, and Z. Li., A new parameterization for the determination of solar flux absorbed at the surface from satellite measurements, *J. Clim.*, *8*, 1615–1629, 1995.

McClatchey, R. A., R. W. Fenn, J. E. A. Selby, F. E. Volz, and J. S. Garing, Optical properties of the atmosphere, *Rep. AFCRL-71-0279*, 85 pp., Air Force Cambridge Res. Lab., Cambridge, Mass., 1971.

Monteith, J. L., Solar radiation and productivity in tropical ecosystems, *J. Appl. Ecol.*, *9*, 747–766, 1972.

Myneni, R. B., and B. D. Ganapol, Remote sensing of vegetation canopy photosynthetic and stomatal conductance efficiencies, *Remote Sens. Environ.*, *42*, 217–238, 1992.

Pinker, R., and I. Laszlo, Modelling surface solar irradiance for satellite applications on a global scale, *J. Appl. Meteorol.*, *31*, 194–211, 1992.

Pokrant, H., *Land Cover Map of Canada Derived From AVHRR Images*, Manitoba Remote Sens. Cent., Ottawa, Ontario, Canada, 1991.

Robertson, B., A. Erickson, J. Friedel, B. Guindon, T. Fisher,

R. Brown, P. Teillet, M. D'Iorio, J. Cihlar, and A. Sancz, GEOCOMP, A NOAA AVHRR geocoding and compositing system, *Proc. ISPRS Conf. Comm.*, *2*, 223–228, 1992.

Roujean, J.-L., and F.-M. Breon, Estimating PAR absorbed by vegetation from bidirectional reflectance measurements, *Remote Sens. Environ.*, *51*, 375–384, 1995.

Roujean, J. L., M. Leroy, A. Leroy, and P. Y. Deschamps, A bidirectional reflectance model of the Earth's surface for the correction of remote sensing data, *J. Geophys. Res.*, *97*, 20,455–20,468, 1992.

Sellers, P. J., Canopy reflectance, photosynthesis and transpiration, *Int. J. Remote Sen.*, *6*, 1335–1372, 1985.

Sellers, P., et al., The boreal ecosystem-atmosphere study (BOREAS): An overview and early results from the 1994 field year, *Bull. Am. Meteorol. Soc.*, *76*, 1549–1577, 1995.

Stephens, G. L., Optical properties of eight water cloud types, *Tech. Pap. 6*, 35 pp., CSIRO Div. of Atmos. Sci., Melbourne, Australia, 1979.

Suttles, J. T., R. N. Green, P. Minnis, G. L. Smith, W. F. Staylor, B. A. Wielicki, I. J. Walker, D. F. Young, V. R. Taylor, and L. L. Stowe, Angular radiation models for Earth-atmosphere system, vol. 1 1, Shortwave radiation, *NASA Ref. Publ. 1184*, 114 pp., 1988.

World Climate Program (WCP), *A Preliminary Cloudless Standard Atmosphere for Radiation Computation*, *WCP-112*, Assoc. for Meteorol. and Atmos. Phys. Radiat. Comm., Geneva, 1986.

Wu, A., Z. Li, and J. Cihlar, Effects of land cover type and greenness on advanced very high resolution radiometer bidirectional reflectances: Analysis and removal. *J. Geophys. Res.*, *100*, 9179–9192, 1995.

J. Cihlar and Z. Li, Canada Centre for Remote Sensing, 588 Booth Street, Ottawa, Ontario, Canada K1A 087. (e-mail: li@ccrs.emr.ca)

L. Moreau, Intermap Information Technologies Ltd., Ottawa, Canada.

(Received April 2, 1996; revised March 3, 1997;
accepted April 24, 1997.)